



## ORIGINAL ARTICLE

# Preparation, characterization, and antitumor activity of *Chaenomeles speciosa* polysaccharide-based selenium nanoparticles



Linan Zhou<sup>a</sup>, Yeling Li<sup>a</sup>, Xiaotang Gong<sup>a</sup>, Zhengguo Li<sup>a</sup>, Honglin Wang<sup>a</sup>,  
Lingling Ma<sup>a</sup>, Muhetaer Tuerhong<sup>b</sup>, Munira Abudukeremu<sup>b</sup>, Yasushi Ohizumi<sup>c</sup>,  
Jing Xu<sup>a,\*</sup>, Yuanqiang Guo<sup>a,\*</sup>

<sup>a</sup> State Key Laboratory of Medicinal Chemical Biology, College of Pharmacy, and Tianjin Key Laboratory of Molecular Drug Research, Nankai University, Tianjin 300350, People's Republic of China

<sup>b</sup> College of Chemistry and Environmental Sciences, Laboratory of Xinjiang Native Medicinal and Edible Plant Resources Chemistry, Kashgar University, Kashgar 844000, People's Republic of China

<sup>c</sup> Kansei Fukushi Research Institute, Tohoku Fukushi University, Sendai 989-3201, Japan

Received 2 March 2022; accepted 21 April 2022

Available online 5 May 2022

## KEYWORDS

Selenium nanoparticles;  
Antitumor;  
*Chaenomeles speciosa*  
polysaccharide;  
Zebrafish

**Abstract** Nanoparticles have been found to possess unique advantages in many fields, especially in the field of cancer treatment. Herein, based on the unique physical and chemical properties of natural polysaccharides, the polysaccharide from the edible and medicinal fruits of *Chaenomeles speciosa* was prepared, and the complex nanoparticles constructed by combining *C. speciosa* polysaccharide with selenium have been successfully developed by a chemical method. Monodisperse spherical nanoparticles with the particle size of 80.5 nm were characterized by various methods, which exhibited ideal size distribution and prominent stability under physiological conditions and alkaline conditions. Cellular studies demonstrated the nanoparticles significantly inhibited the growth of MCF-7 cells with an IC<sub>50</sub> value of 8.37 ± 0.97 μg/mL through inducing the apoptosis and arresting the cell circle at S phase. Moreover, the zebrafish assays confirmed the antitumor effects of the nanoparticles, which suppressed the proliferation and migration of tumor and blocked the angiogenesis of transgenic zebrafish. Collectively, the results suggested that the nanoparticles may be considered as a candidate agent to treat breast cancer.

© 2022 The Author(s). Published by Elsevier B.V. on behalf of King Saud University. This is an open access article under the CC BY-NC-ND license (<http://creativecommons.org/licenses/by-nc-nd/4.0/>).

\* Corresponding authors.

E-mail addresses: [xujing611@nankai.edu.cn](mailto:xujing611@nankai.edu.cn) (J. Xu), [xujing611@nankai.edu.cn](mailto:xujing611@nankai.edu.cn), [victgyq@nankai.edu.cn](mailto:victgyq@nankai.edu.cn), [victgyq@nankai.edu.cn](mailto:victgyq@nankai.edu.cn) (Y. Guo).

Peer review under responsibility of King Saud University.



## 1. Introduction

Breast cancer is a heterogeneous and complex disease, which is considered to be one of the most prevalent cancers in the world. The traditional therapeutic modalities for breast cancer comprise chemotherapy, radiotherapy, and immunotherapy. Among them, chemotherapy is the most commonly used method to treat breast cancer. However, most chemotherapy drugs have poor tumor targeting and narrow treatment window, which inevitably cause serious toxicity and side effects, resulting in poor quality of life of cancer patients (Ma et al., 2020). In recent years, nanomedicine and related nanoparticles based on biomaterials have attracted special attention, which have been proved to be very helpful in improving cancer treatment and avoiding toxic side effects (Shi et al., 2017; Pandit et al., 2020). Up to date, nanomedicine has been considered as a promising strategy to achieve desirable antitumor effects, which prompts us to develop new nanoparticles to alleviate the pressure of tumor treatment (Liu et al., 2018, 2022a; Wang et al., 2019; Wang and Luo, 2019; Xu et al., 2022; Yang et al., 2021a).

As a trace element with multiple biological functions, selenium (Se) is of great significance in maintaining redox balance, immune regulation, anticancer, etc. (Xia et al., 2021; Yang et al., 2021b; Zhang et al., 2022). Selenium deficiency can damage the immune system and increase the risk of cancer (Tang et al., 2021). In addition, the chemical valence of selenium has an important influence on its bioavailability and biological functions. Recently, selenium nanoparticles (SeNPs) existing as zero valent state, have drawn more and more attention for their high biological activity and low toxicity (Yan et al., 2021; Qiao et al., 2020; Wang et al., 2019; Song et al., 2021). Zhang et al. reported that SeNPs can induce tumor cell apoptosis by triggering apoptosis signal transduction pathway (Zhang et al., 2013). Therefore, SeNPs are considered to be not only selenium supplementations but also potential agents for cancer chemoprevention and chemotherapy. Nevertheless, the application of SeNPs as an antitumor agent has some urgent problems to be solved, such as poor stability and low bioavailability, which hinders its medical application.

As distinctive natural materials, polysaccharides have been attracting extraordinary interest for their attractive characteristics, such as nontoxicity, hydrophilicity, and high compatibility, which are pivotal characteristics, while considering a material for biomedical applications (Zeng et al., 2021; Wusigale et al., 2021; Hu et al., 2021). When compared with other biomolecules, polysaccharides have many functional groups including hydroxy, amino, and carboxyl groups, which make them easy to modify and can be used to prepare a variety of new biological nanostructures (Li et al., 2021a). Additionally, most polysaccharides have inherent immunomodulatory and antioxidant effects (Zhang et al., 2021a,a; Zhou et al., 2020). Hence, polysaccharides are regarded as biomaterials with remarkable tunable properties. Recently, polysaccharide-based nano-preparations have been booming in cancer treatment (Cao et al., 2021). Some polysaccharides combined with nanotechnology, such as *Gracilaria lemaneiformis* polysaccharides and mushroom polysaccharides, have achieved excellent biological effects (Zeng et al., 2019). *Chaenomeles speciosa* (Sweet) Nakai. belongs to the Rosaceae family and its fruits are edible and medicinal, which are rich in polysaccharides and have been

reported to be nutritional and have numerous pharmacological effects (Xie et al., 2015). To date, although some polysaccharides and their biological effects from *C. speciosa* were reported (Xie et al., 2015; Cheng et al., 2020), there have been no reports to use the polysaccharides in *C. speciosa* as biomaterials. Considering the edible and medicinal value of the fruits of *C. speciosa*, its polysaccharides may be utilized as biomaterials to combine with selenium nanoparticles to afford polysaccharide-selenium nanoparticles, which give full play to their respective advantages and overcome the application limitations of selenium nanoparticles and polysaccharides.

As mentioned above, this work plans to design and prepare a new type of polysaccharide-based selenium nanoparticles as an anti-breast cancer agent by combining natural polysaccharides with selenium. In addition to optimizing the parameters for preparing nanoparticles, the physicochemical properties, the stability under physiological conditions, and the formation mechanism of the nanoparticles obtained were systematically investigated. As an exploration of the prepared nanoparticles against breast cancer, the antitumor activity and preliminary mechanism were also examined using cell and zebrafish models.

## 2. Materials and methods

### 2.1. Materials and reagents

Materials and reagents are supplemented in the Supporting Information.

### 2.2. Preparation and characterization of *C. speciosa* polysaccharide (CSP)

#### 2.2.1. Extraction of CSP

The polysaccharide CSP from the dried fruits of *C. speciosa* was prepared using the reported method (Li et al., 2021b). The preparation process and detailed method are supplemented in the Supporting Information.

#### 2.2.2. Chemical composition of CSP

To clarify the ingredients of the CSP, the contents of polysaccharides, proteins and uronic acids were evaluated (Barbosa et al., 2009; Cesaretti et al., 2003; Zhang et al., 2020b; Dubois et al., 1956). The ultraviolet full wavelength scanning was used to detect the residue of protein and nucleic acid of CSP at the range of 200–400 nm.

#### 2.2.3. Monosaccharide composition analysis of CSP

The monosaccharide composition of CSP was analyzed by the 1-phenyl-3-methyl-5-pyrazolone (PMP) method (Honda et al., 1989). The details are described in the Supporting Information.

#### 2.2.4. Thermogravimetric analysis of CSP

The thermogravimetric analysis (TGA) of CSP was performed at TGA/DSC1 (Mettler Toledo) as the previous report (Nawrocka et al., 2017). CSP sample (8 mg) was put in an alumina pan and heated from 30 °C to 600 °C. Nitrogen was used as the carrier gas to heat the sample. The experimental process was monitored and the decomposition temperature and weight

loss were calculated using Origin software (Version 9.0 PRO, OriginLab Corporation, USA).

### 2.3. Preparation of CSP-SeNPs

Four types of CSP-SeNPs with various selenium content were constructed using the previous method (Zhang et al., 2021b). Briefly, Tween 80 solution (4 mL, 10 mg/mL) was added dropwise to 5 mL of sodium selenite solution (20, 40, 80, and 120 mM) under stirring. Subsequently, CSP solution (8 mL, 10 mg/mL) was mixed with the above solution and stirred for 1 h. Then, 3 mL of the freshly prepared ascorbic acid with different concentrations (100, 200, 400, and 600 mM) was added dropwise into the mixed solution under dark conditions and then stirred vigorously for another 24 h at room temperature, respectively. After reaction, the solution was dialyzed for 72 h ( $M_w$  cut-off, 3500 Da). The obtained four selenium nanoparticles solutions were labeled in order as CSP-SeNP1, CSP-SeNP2, CSP-SeNP3, and CSP-SeNP4.

### 2.4. Characterization of CSP-SeNPs

The particle size, zeta potential, and polydispersity index (PDI) of CSP-SeNPs were measured by a nanoparticle analyzer (Nano ZS, Malvern, UK). The Fourier transform-infrared spectrum (FT – IR) of CSP-SeNPs was obtained with a FT – IR spectrometer (Bruker Optics, Ettlingen, Germany) in the range of 4000–400  $\text{cm}^{-1}$ . The morphology of CSP-SeNPs was observed by transmission electron microscopy (TEM, Talos F200C, FEI, USA). A field emission scanning electron microscope (FE-SEM, JEOL-JSM-7800F, Tokyo, Japan) was utilized to determine the element distribution in CSP-SeNPs.

### 2.5. Stability of CSP-SeNP3

The storage stability of CSP-SeNP3 in water, DMEM, and DMEM containing 10% (v/v) fetal bovine serum (FBS) was investigated. The particle size and PDI of CSP-SeNP3 solution were measured regularly by dynamic light scattering (DLS). The pH value of CSP-SeNP3 solution was adjusted between 2 and 12 by hydrochloric acid or sodium hydroxide. The effects of pH and time on the particle size stability of CSP-SeNP3 were also evaluated (Zhang et al., 2018).

### 2.6. Antitumor activity evaluation of CSP-SeNP3

#### 2.6.1. Cell and zebrafish

The cell culture (A549, MCF-7, and HepG2) and the maintenance and breeding of zebrafish (AB strain and *Tg(fli1:EGFP)* transgenic zebrafish) were carried out as described in the Supporting Information.

#### 2.6.2. Cellular antitumor effects of CSP and CSP-SeNP3

The cellular antitumor effects of CSP and CSP-SeNP3 were detected by MTT assay. In short, after seeding cells into a 96-well plate ( $5 \times 10^3$  cells/well) and incubation for 24 h, various concentrations of CSP or CSP-SeNP3 were added and incubated continuously for 48 h. Subsequently, 20  $\mu\text{L}$  MTT

solution (5 mg/mL) was added and the incubation of 4 h was performed. After removing the supernatants, the formazan crystals at the bottom were dissolved with DMSO, and the absorbance was measured (Thermo Fisher Scientific, Waltham, MA, USA).

#### 2.6.3. Analysis for cell apoptosis

Analysis for MCF-7 cell apoptosis induced by CSP-SeNP3 was conducted by flow cytometry using Annexin V-FITC Apoptosis Detection Kit (Beyotime, C1062L) (Zhang et al., 2021d). After being treated with different concentrations of CSP-SeNP3 (0.8, 4, and 20  $\mu\text{g}/\text{mL}$ ), the MCF-7 cells were washed twice with PBS and resuspended in the binding buffer (Beyotime, Shanghai, China). Then, 5  $\mu\text{L}$  of Annexin V-FITC and 10  $\mu\text{L}$  of propidium iodide (PI) were added, and the solution were incubated for 20 min at room temperature in the dark. The apoptosis was detected by BD LSRFortessa flow cytometry (BD Biosciences), and data were obtained by FLOWJO software (FLOWJO LLC, Ashland, OR, USA).

#### 2.6.4. Analysis for cell cycle

The cell cycle distributions of MCF-7 cells affected by CSP-SeNP3 were evaluated by flow cytometry (Guo et al., 2021). MCF-7 cells in exponential growth phase were inoculated in 12-well plates ( $2 \times 10^5$  cells/well) for 24 h. After treated with different concentrations of CSP-SeNP3 (0.4, 2, and 10  $\mu\text{g}/\text{mL}$ ) and incubated for 48 h, MCF-7 cells were collected, washed twice with PBS, and fixed overnight in 70% cold ethanol at 4 °C. Then, the cells were washed and stained with propidium iodide staining buffer containing RNase (Beyotime, C1052) for 30 min at 37 °C in the dark. The cellular DNA analysis was performed immediately by flow cytometry and the data were processed using ModFit LT Software.

#### 2.6.5. In vivo antitumor evaluation with a zebrafish model

The normal embryos at 48 h post-fertilization (hpf) from adult AB zebrafish were selected for *in vivo* antitumor evaluation using the method reported (Zhang et al., 2021c). Briefly, 5 nL ( $1 \times 10^7$  cells/mL) of stained MCF-7 cells by CM-DiI (2.5  $\mu\text{M}$ ) were microinjected into the yolk sac of zebrafish embryos. After incubation of 4 h at 28.5 °C, the tumor cell-bearing embryos were stochastically classified into groups (15 embryos/group) and various concentrations (0.5, 1, and 2  $\mu\text{g}/\text{mL}$ ) of CSP-Tw-SeNP3 or etoposide (positive control) were added for continuous incubation of 48 h. At 5 days post-fertilization (dpf), the zebrafish embryos were observed by confocal microscopy (Leica, Germany), and the density and focus of red fluorescence representing the proliferation and migration of MCF-7 cells were statistically analyzed by ImageJ (NIH, Bethesda, MD, USA).

#### 2.6.6. Anti-angiogenesis assay of CSP-SeNP3

The anti-angiogenesis experiments were performed using transgenic zebrafish *Tg(fli1:EGFP)* embryos (Li et al., 2021c). Briefly, normal embryos (6 hpf) were selected and treated by CSP-SeNP3 for 48 h. Intersegmental vessels (ISVs) of the treated embryos were observed and photographed. ImageJ software (NIH, Bethesda, MD, USA) was used for quantitative analysis of the total average length of the ISVs.

## 2.7. Statistical analysis

GraphPad Prism 7.0 software (GraphPad Software Inc., La Jolla, CA) was used for the data processing. One-way ANOVA and Tukey's multiple comparison test were employed for the differences.

## 3. Results and discussion

### 3.1. Chemical characterization of CSP

#### 3.1.1. Chemical composition of CSP

The polysaccharide CSP was extracted and prepared from the dry fruits of *C. speciosa*. The percentage content of the carbohydrate, protein, and uronic acid were 96.58%, 7.89%, and 0.66%, respectively. As illustrated in Fig. S1, an unobvious peak at 280 nm was shown in the UV spectrum of CSP, implying that CSP contained a small amount of protein, which was consistent with the result of protein content analysis. Meanwhile, there was no signal around 260 nm, indicating the absence of nucleic acid. The monosaccharide composition analysis of CSP was presented in Fig. 1A, the result revealed that CSP mainly was composed of three kinds of monosaccharides including galacturonic acid, galactose, and arabinose.

#### 3.1.2. Thermal analysis

The thermogravimetric analysis (TGA) was used to detect the stable of polysaccharide. As shown in Fig. 1B, the process of weight loss occurred three times during the heating-up phase, which was related to the stability of the polysaccharide (Kumar Varma and Jayaram Kumar, 2017). The first mass loss of about 6.0% occurred in the range of 31.4 to 202.9 °C, which was caused by the loss of water. The second mass loss was 59.0% (202.9–412.9 °C), which was mainly caused by the pyrolysis of polysaccharide skeleton. Differential scanning calorimetry (DSC) curves were shown by two endothermic states at 31.4 °C and 297.2 °C, which indicated that the thermally decomposed temperature of CSP was around 300 °C. Both the results of TGA and DSC analysis revealed that CSP has a stable chemical structure. The good stability implied that CSP may be considered as being a nanocarrier.

### 3.2. Preparation of CSP-SeNPs

The combination of selenium nanoparticles and natural polysaccharides through green strategy may effectively solve the inherent limitations of selenium nanoparticles, which is conducive to further improve the bioavailability and antitumor activity of selenium nanoparticles and expand their potential applications in tumor therapy (Li et al., 2019a). In this study, selenium nanoparticles functionalized by *C. speciosa* polysaccharide (CSP-SeNPs) were prepared by the reaction of sodium selenite and ascorbic acid in the presence of *C. speciosa* polysaccharide. In the preparation reaction, the precursor selenite was first dispersed in the microenvironment of *C. speciosa* polysaccharide, and then the added ascorbic acid reacted with selenite to produce elemental selenium. The elemental selenium produced by the reaction was adsorbed and wrapped in situ by *C. speciosa* polysaccharide, so as to effectively prevent the mutual combination and agglomeration of the initially formed particles, slow down and control the growth of particles, and make the selenium nanoparticles stably exist in the solution (Tang et al., 2019). While, it was found that the application of Tween 80 during the preparation of nanoparticles can prolong the stabilization time of CSP-SeNPs.

### 3.3. Characterization of CSP-SeNPs

#### 3.3.1. Nanoparticle size of CSP-SeNPs

In order to obtain selenium nanoparticles with small particle size and good stability, four types of nanoparticles stabilized by *C. speciosa* polysaccharide (CSP-SeNPs1 – 4) were prepared. As shown in Fig. S2, black SeNPs without CSP surface decoration aggregated at the bottom, while the solution of CSP-SeNPs decorated with CSP was transparent. The stability and dispersion of CSP-SeNPs were significantly improved when compared with bare SeNPs. Besides, the effects of sodium selenite concentration on nanoparticle size and PDI of CSP-SeNPs were investigated. As presented in Fig. 2A, the average diameter and PDI of CSP-SeNPs gradually decreased with the increase of sodium selenite concentration from 5 to 20 mM ( $105.1 \pm 1.7$  nm and 0.214,  $101.9 \pm 4.0$  nm and 0.288,  $80.5 \pm 0.9$  nm and 0.250). However, when the concentration of sodium selenite rose to 30 mM, the aver-

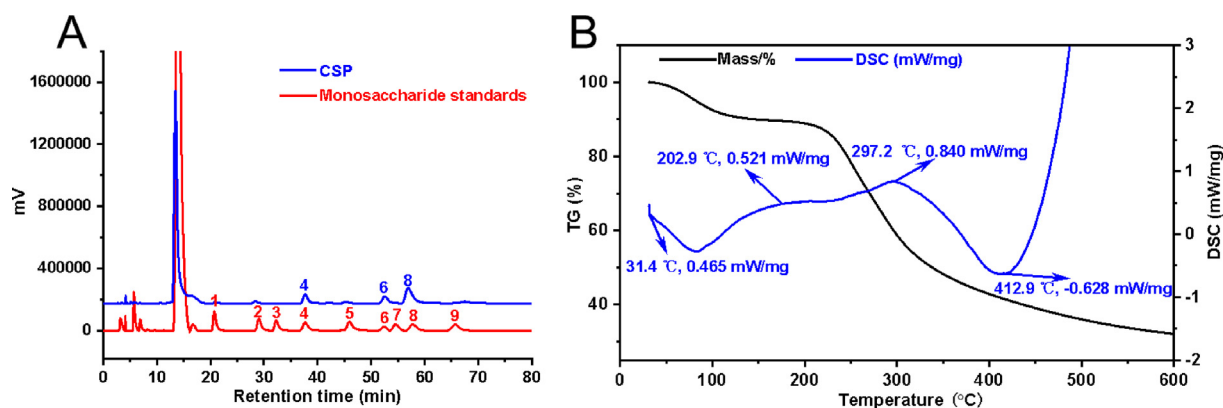


**Fig. 1** Analysis of physicochemical properties of CSP. Monosaccharide composition (A) analysis of CSP (1: mannose; 2: rhamnose; 3: glucuronic acid; 4: galacturonic acid; 5: glucose; 6: galactose; 7: xylose; 8: arabinose; 9: fucose). Thermal gravimetric analysis (TG) and differential scanning calorimetric (DSC) analysis of CSP (B).

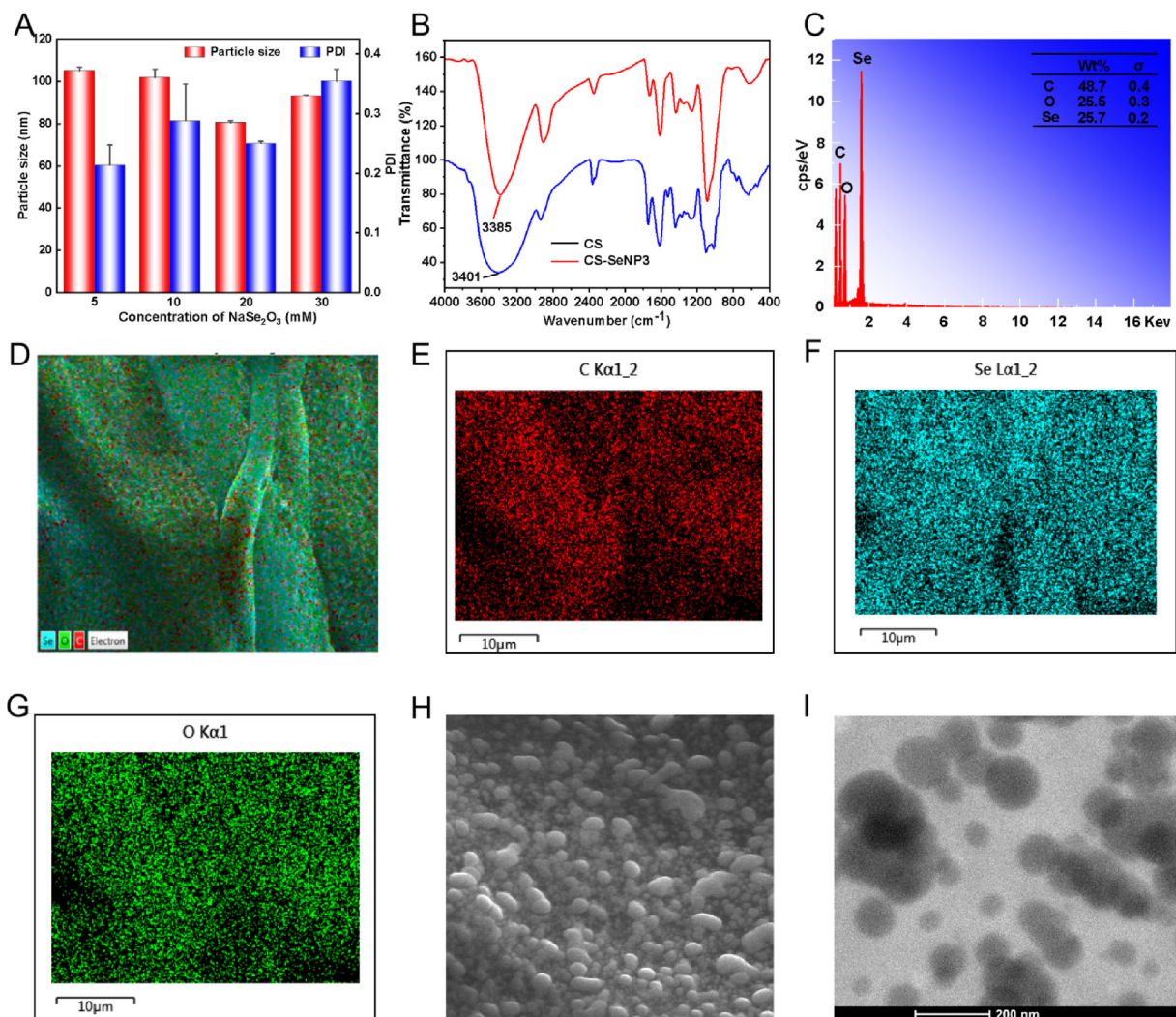


**Fig. 2** Characterization of CSP-SeNPs. The influence of sodium selenite concentration on the particle size and PDI of SeNPs (A). FT – IR spectra of CSP and CSP-SeNPs (B). EDS analysis of CSP-SeNP3 (C – G). SEM image of CSP-SeNP3 (H). TEM image of CSP-SeNP3 (I).

age diameter and PDI of CSP-SeNPs increased to  $93.1 \pm 0.5$  nm and 0.354, respectively. These changes may be that the strong molecular interactions among polysaccharide molecules weakened the binding ability between CSP and SeNPs (Ye et al., 2020). These results showed that 20 mM of sodium selenite seemed to be an optimal concentration with smaller size and ideal PDI. Therefore, CSP-SeNP3 was chosen for the following experiments.

### 3.3.2. Interactions between CSP and SeNPs by FT-IR spectra

The potential interactions between CSP and SeNPs were analyzed from the FT – IR spectra. As shown in Fig. 2B, CSP-SeNP3 have characteristic absorption bands similar to those of CSP, indicating that no new covalent bonds formed (Liao et al., 2016). Moreover, compared with the native polysaccharide of CSP ( $3401 \text{ cm}^{-1}$ ), the absorption band for hydroxy in CSP-SeNP3 was significantly blue-shifted by  $16 \text{ cm}^{-1}$ . The shift implied the strong bond between the hydroxy group of CSP and SeNPs, which was consistent with the previously reported results (Xiao et al., 2017).

### 3.3.3. Element content and surface morphology of CSP-SeNP3

The element composition and surface morphology of CSP-SeNP3 were investigated using FE-SEM with energy dispersive spectroscopy (EDS) and TEM. The SEM images (Fig. 2C – H) showed that CSP-SeNP3 composed of C, O, and Se presented as a spherical solid, which were uniformly doped in CSP-SeNP3 in a proportion of 48.7%, 25.5%, and 25.7%, respectively. The results of elemental composition of polysaccharide-based SeNPs were similar with those reported in the literature, such as *Lycium barbarum* polysaccharide-SeNPs (Liu et al., 2021), dandelion polysaccharide-SeNPs (Zhang et al., 2021b), and *Citrus limon* polysaccharide-SeNPs (Zhou et al., 2021). The subsequent TEM detection showed that CSP-SeNP3 displayed a spherical morphology with excellent dispersion (Fig. 2I).

### 3.4. Stability of CSP-SeNP3

The nanoparticle stability under physiological conditions is the key index to determine whether they can be practically applied

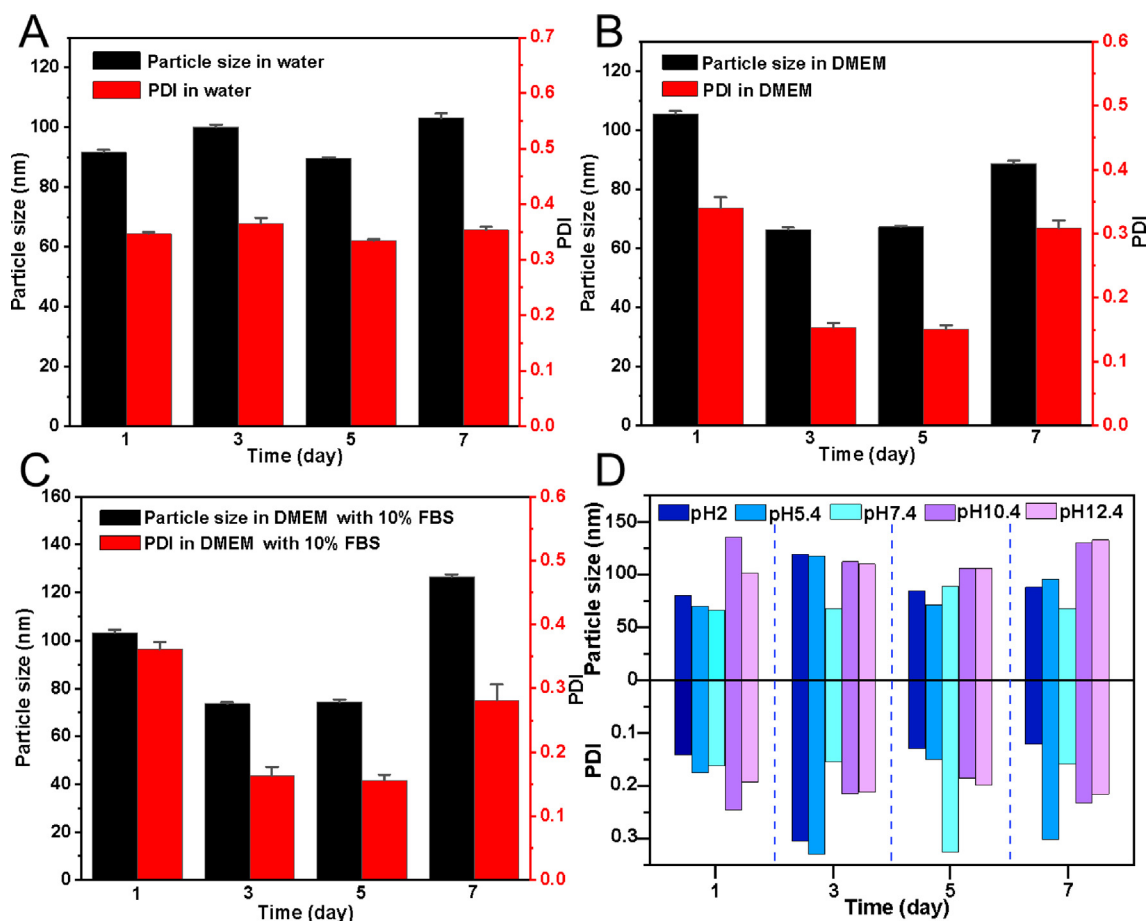


**Fig. 3** Stability analysis of CSP-SeNP3. The changes of particle size and PDI of CSP-SeNP3 in water (A), DMEM (B) and DMEM containing 10% FBS (C) for 7 days. The influence of pH on the stability of CSP-SeNP3 during 7 days of storage (D).

(Li et al., 2010). To investigate the applicability of CSP-SeNP3, CSP-SeNP3 were suspended in water, DMEM, and DMEM added with 10 % (v/v) FBS for 7 days, respectively. As presented in Fig. 3A-C, the nanoparticle size of CSP-SeNP3 in DMEM added with 10 % (v/v) FBS increased to around 126.6 nm on the 7th day, while the nanoparticle diameter of CSP-SeNP3 exhibited negligible changes on the 7th day when the CSP-SeNP3 suspended in water and DMEM. These results indicated that the excellent stability of CSP-SeNP3 under physiological conditions. As depicted in Fig. 3D, the nanoparticle size of CSP-SeNP3 under acidic conditions (pH = 2.0 and 4.4) increased slightly and showed instability compared with those under alkaline conditions (pH = 10.4 and 12.4), implying that the pH also had a significant effect on the size of CSP-SeNP3. The experiments of pH changes suggested the acidic conditions may destroy the interactions between CSP and SeNPs and lead to the aggregation of nanoparticles (Liu et al., 2021).

### 3.5. *In vitro* and *in vivo* antitumor activity of CSP-SeNP3

#### 3.5.1. *In vitro* antitumor assay of CSP and CSP-SeNP3

The *in vitro* antitumor effects of CSP and CSP-SeNP3 on MCF-7, HepG2, and A549 cell lines were detected by MTT assay. As shown in Fig. 4A – C, CSP exhibited negligible cyto-

toxicity toward three cancer cells in the concentration range of 1–100  $\mu\text{g}/\text{mL}$ , while CSP-SeNP3 significantly inhibited proliferation of three cancer cells dose-dependently. The antitumor effects of CSP-SeNP3 were comparable with the inhibitory effects of LAG-SeNPs on A549, MCF-7, and HepG2 cells (Tang et al., 2019; Li et al., 2019b). The strong inhibitory effects and  $\text{IC}_{50}$  values indicated that CSP-SeNP3 possessed broad-spectrum inhibition against cancer cells and had promising application in the field of cancer chemotherapy.

#### 3.5.2. Apoptosis effects induced by CSP-SeNP3

To examine the possible inhibitory mechanism of CSP-SeNP3 to tumor cells, the apoptosis of MCF-7 cells treated with different concentrations of CSP-SeNP3 (0.8, 4, and 20  $\mu\text{g}/\text{mL}$ ) was assessed by Annexin V-FITC/PI double staining experiments. As shown in Fig. 5A and 5C, the regions Q2 and Q3 represented the cell apoptosis. With the increase of CSP-SeNP3 concentration, the apoptotic proportion in Q2 and Q3 regions was ascended from 21.79% (0.8  $\mu\text{g}/\text{mL}$ ) to 22.08% (4  $\mu\text{g}/\text{mL}$ ) and 28.09% (20  $\mu\text{g}/\text{mL}$ ), indicating that CSP-SeNP3 promoted apoptosis dose-dependently. Similar results were reported in the previous research, in which the selenium nanoparticles stabilized by laminarin polysaccharides (LP-SeNPs) had a significant effect of apoptosis induction (Cui et al., 2019).

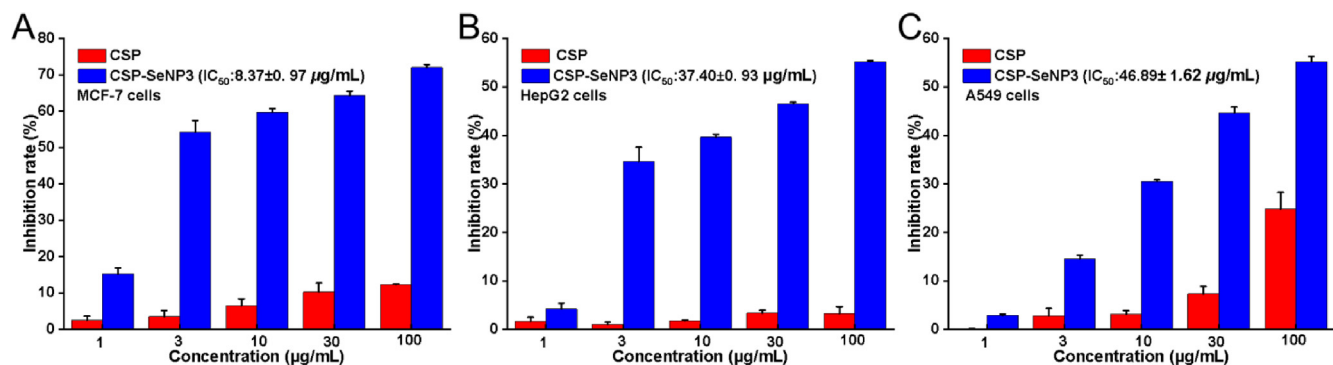


**Fig. 4** Inhibition rates of CSP and CSP-SeNP3 on tumor cells. Inhibition rates of CSP and CSP-SeNP3 on MCF-7 cells (A). Inhibition rates of CSP and CSP-SeNP3 on HepG2 cells (B). Inhibition rates of CSP and CSP-SeNP3 on A549 cells (C). Data from three separate experiments are expressed as means ± SD.

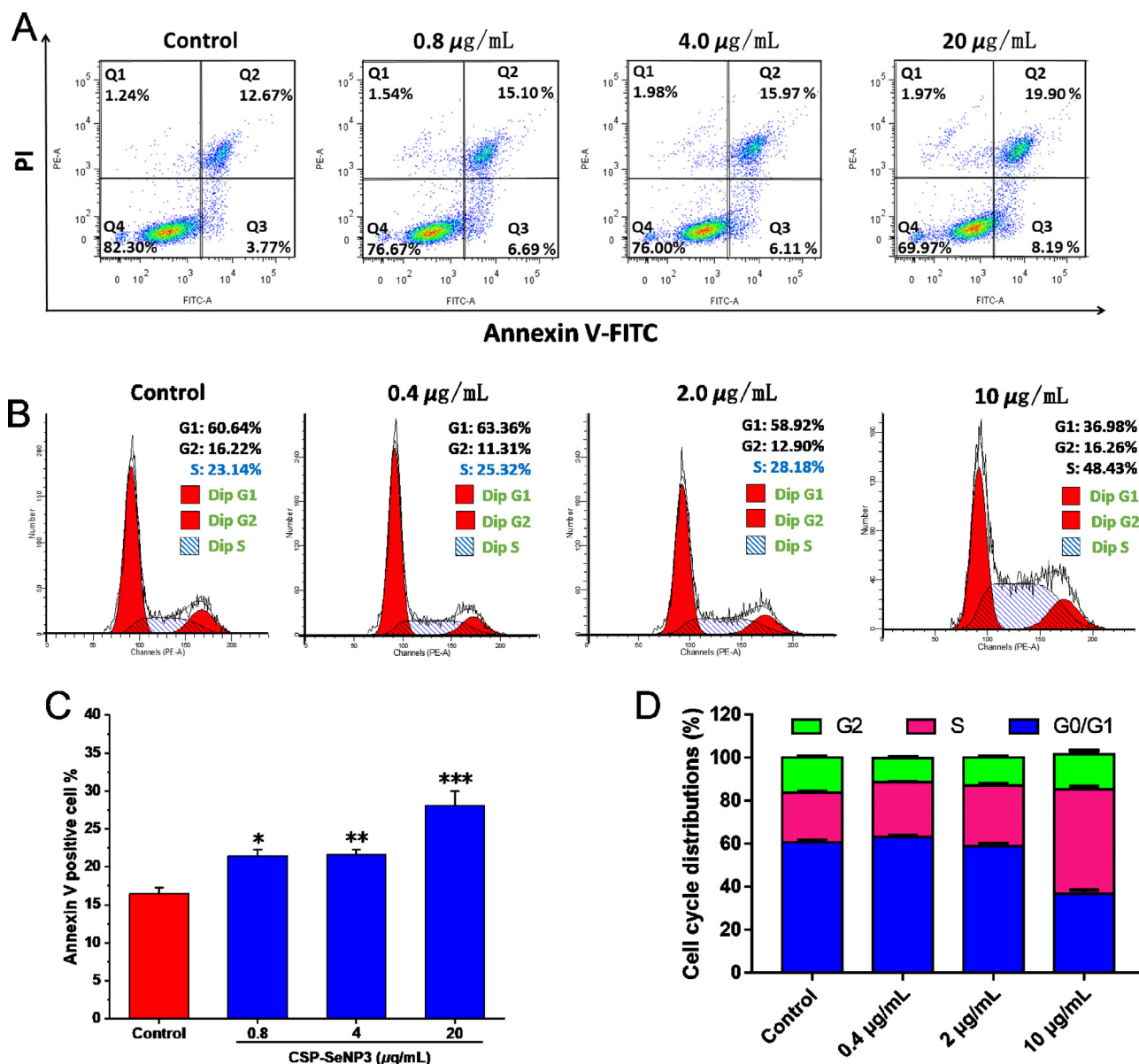


**Fig. 5** Apoptosis and cell cycle determination results of CSP-SeNP3-treated MCF-7 cells. Flow cytometric analysis of MCF-7 cells after treated with different concentrations of CSP-SeNP3 (A). Cell cycle distributions of MCF-7 cells after treated with different concentrations of CSP-SeNP3 (B). Histogram of apoptotic cells at 48 h with the treatment of CSP-SeNP3 (C). Data processing of cell cycle distribution (D). Data from three separate experiments are expressed as means ± SD. \* $P < 0.05$ , \*\* $P < 0.01$ , and \*\*\* $P < 0.001$  vs. control group.

### 3.5.3. Effects of CSP-SeNP3 on cell cycle

Cell apoptosis is closely coupled with cell cycle (Liu et al., 2022b). The cell cycle distributions of MCF-7 cells affected by CSP-SeNP3 (0.4, 2, and 10  $\mu\text{g}/\text{mL}$ ) were detected by flow cytometry. As presented in Fig. 5, the proportions of cells in S phase after CSP-SeNP3 treatments were obviously ascended from 25.32% to 48.43%, while the percentages in G0/G1 phase were decreased, which indicated that CSP-SeNP3 induced MCF-7 cell apoptosis via cell cycle arrest at S phase. The results were similar with those of the selenium nanoparticles modified by *Codonopsis pilosula* polysaccharide (CPP-SeNPs), which also induced HepG2 cell apoptosis by arresting cell cycle at S phase (Yu et al., 2022).

### 3.5.4. In vivo antitumor activity of CSP-SeNP3

The *in vitro* experiments showed that CSP-SeNP3 emerged promising antitumor effects. To further explore the anti-proliferation and anti-metastasis potential of CSP-SeNP3 *in vivo*, a zebrafish tumor xenograft model was employed, in which fluorescent labeled MCF-7 cells were microinjected into zebrafish embryos. As shown in Fig. 6, the relative intensity

and foci of red fluorescence representing tumor proliferation and metastasis (Li et al., 2021c), respectively, were reduced dose-dependently, showing that CSP-SeNP3 had significant *in vivo* antitumor effects. From the results shown in Fig. 6, the relative intensity and foci of red fluorescence at CSP-SeNP3 concentration of 2  $\mu\text{g}/\text{mL}$  were significantly lower than that of etoposide, suggesting that the inhibitory effect of CSP-SeNP3 at this concentration was better than that of the positive control group. These results exhibited that CSP-SeNP3 had strong antitumor effects in the established zebrafish model.

### 3.5.5. Angiogenesis inhibitory effects of CSP-SeNP3

Tumor proliferation and metastasis are coupled with angiogenesis. To examine whether the *in vivo* antitumor effects of CSP-SeNP3 are related with the inhibition of angiogenesis, a transgenic zebrafish *Tg(fli1:EGFP)* model was utilized, in which the newly formed vessels presented green fluorescence to observe easily (Li et al., 2021c). As depicted in Fig. 7A, treatment with CSP-SeNP3, the intersegmental vessels (ISVs) of zebrafish embryos were obviously broken, and the average

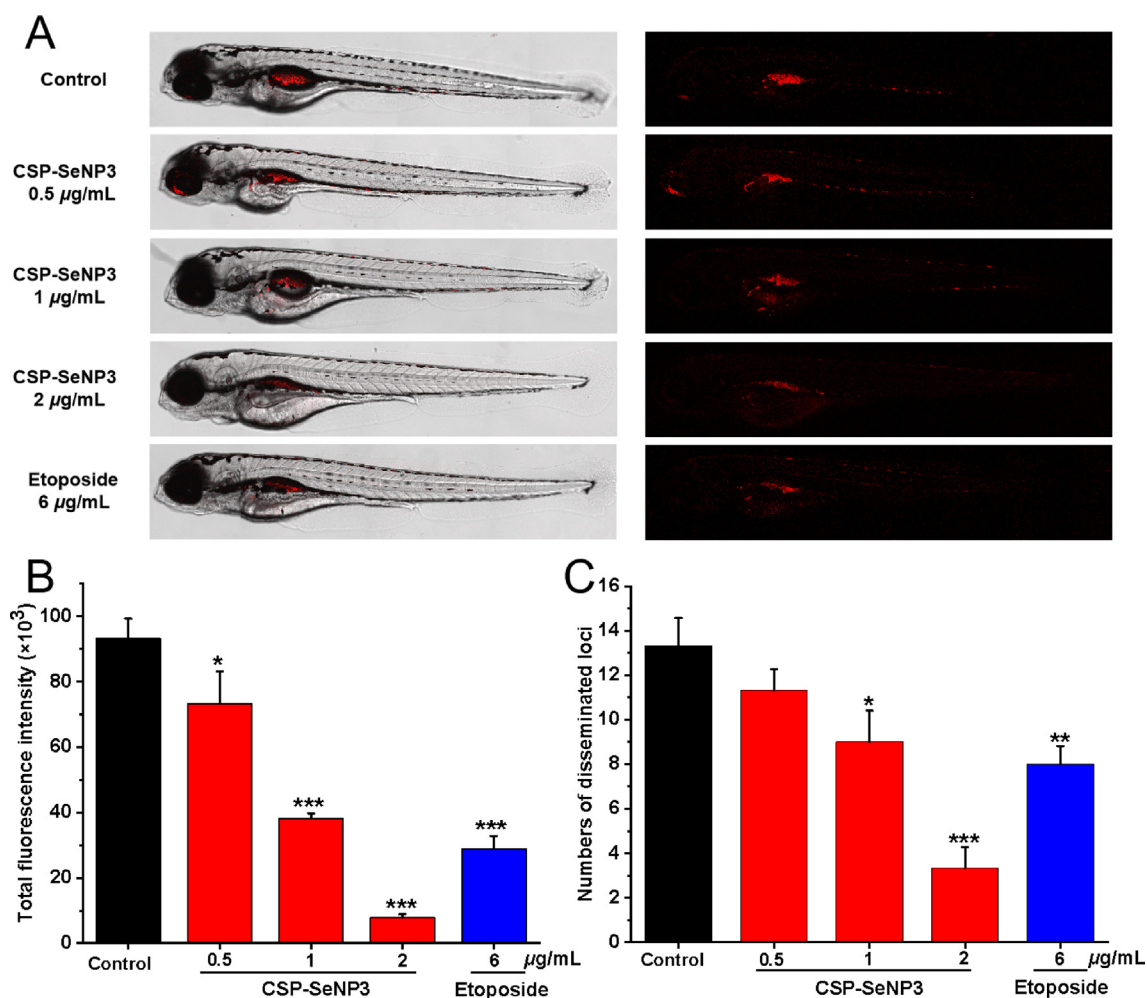


**Fig. 6** Inhibitory effects of CSP-SeNP3 on the proliferation and migration of MCF-7 cells in zebrafish. Intensity and distribution of the red fluorescence (A) were imaged under a confocal microscope in zebrafish larvae at 5 dpf ( $n = 15/\text{group}$ ). Tumor proliferation (B) and metastasis (C) were quantified using Image J software. All values are expressed as the mean  $\pm$  SD of at least three independent experiments. \* $P < 0.05$ , \*\* $P < 0.01$ , \*\*\* $P < 0.001$  vs. the control group.

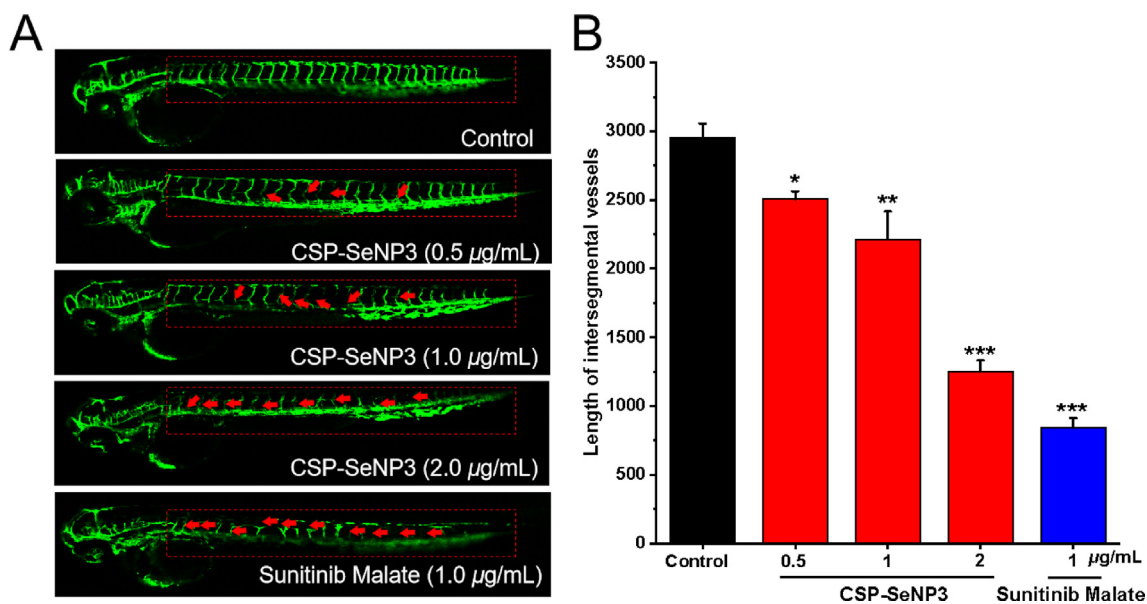


**Fig. 7** Anti-angiogenesis activity of CSP-SeNP3 in the transgenic zebrafish model. Representative images of *Tg(fli1:EGFP)* zebrafish embryos (A) at 48 hpf treated various concentrations of CSP-SeNP3 (0.5, 1, and 2 µg/mL) under live fluorescence microscopy. The absence and break of ISVs were indicated by red arrows. The length of ISVs of zebrafish (B) after treated with different concentrations of CSP-SeNP3 (0.5, 1, and 2 µg/mL). (n = 15 for each experimental group). \* $P < 0.05$ , \*\* $P < 0.01$ , and \*\*\* $P < 0.001$  vs. control group.

length of ISVs in zebrafish embryos was further analyzed quantitatively (Fig. 7B). According to the statistical analysis, the average length of ISVs was  $1250.6 \pm 82.5 \mu\text{m}$  at the concentration of 2 µg/mL, which was significantly decreased when compared with that of the blank control group ( $2955.8 \pm 101.9 \mu\text{m}$ ). The experiments demonstrated that CSP-SeNP3 could significantly suppress angiogenesis *in vivo*. Angiogenesis is bound up with the occurrence, development, invasion, and metastasis of tumor (Ferrara et al., 2003), and the inhibition of angiogenesis can prevent tumor growth. The angiogenic experiments showed that CSP-SeNP3 might be used as an angiogenesis inhibitor in tumor therapy.

#### 4. Conclusions

In the present study, a kind of *C. speciosa* polysaccharide-based selenium nanoparticles was successfully designed and prepared for the possible applications against breast cancer. The nanoparticles formed under the optimized conditions presented monodisperse and homogeneous spherical structure and the hydrodynamic size was 80.5 nm. FT-IR analysis indicated the formation of the nanoparticles may be due to the strong interactions between the hydroxy group of *C. speciosa* polysaccharide and bare selenium nanoparticles. The nanoparticles exhibited superior colloid stability in physiological and alkaline solution. The *in vitro* cell assays demonstrated that the nanoparticles could effectively inhibit tumor cells by prompting cell apoptosis and blocking cell cycle at S phase. The further *in vivo* antitumor experiments using the zebrafish model indicated that the prepared nanoparticles CSP-SeNP3 effectively blocked tumor proliferation and metastasis, for which the antitumor effects were comparable with that of etoposide. As a further exploration of possible antitumor mechanism, the prepared nanoparticles CSP-SeNP3 were found to suppress zebrafish angiogenesis in a dose-dependent

manner in the transgenic zebrafish model. In general, the current work has prepared *C. speciosa* polysaccharide-based selenium nanoparticles with good stability, which provides a possible solution to the application limitations of bare selenium nanoparticles. While, the good activity of nanoparticles *in vivo* and *in vitro* showed that the polysaccharide-based selenium nanoparticles may have a great prospect for the treatment of breast cancer.

#### CRedit authorship contribution statement

**Linan Zhou:** Methodology, Data curation, Investigation, Software, Writing – original draft. **Yeling Li:** Methodology, Data curation, Investigation, Software. **Xiaotang Gong:** Methodology, Data curation, Investigation, Software. **Zhengguo Li:** Methodology, Data curation, Investigation, Software. **Honglin Wang:** Methodology, Data curation, Investigation. **Lingling Ma:** Methodology, Data curation, Investigation. **Muhetaer Tuerhong:** Writing – Review & editing. **Munira Abudukeremu:** Writing – Review & editing. **Yasushi Ohizumi:** Writing – Review & editing. **Jing Xu:** Conceptualization, Funding acquisition, Project administration, Methodology, Supervision. **Yuanqiang Guo:** Conceptualization, Funding acquisition, Project administration, Methodology, Supervision.

#### Declaration of Competing Interest

The authors declare that they have no known competing financial interests or personal relationships that could have appeared to influence the work reported in this paper.

#### Acknowledgments

This research was supported financially by the National Natural Science Foundation of China (Nos. 22177054, U1801288,

22077067, and 21864016), the Scientific Research Program of the Higher Education Institution of Xinjiang Uygur Autonomous Region (No. XJEDU20171010), and the Natural Science Foundation of Tianjin, China (No. 19JCYBJC28100).

## Appendix A. Supplementary data

Supplementary data to this article can be found online at <https://doi.org/10.1016/j.arabjc.2022.103943>.

## References

- Barbosa, H., Slater, N., Marcos, J.C., 2009. Protein quantification in the presence of poly (ethylene glycol) and dextran using the Bradford method. *Anal. Biochem.* 395, 108–110.
- Cao, B., Zhang, Q., Guo, J., Guo, R., Fan, X., Bi, Y., 2021. Synthesis and evaluation of *Grateloupia Livida* polysaccharides-functionalized selenium nanoparticles. *Int. J. Biol. Macromol.* 191, 832–839.
- Cheng, X., Shi, S., Su, J., Xu, Y., Ordaz-Ortiz, J.J., Li, N., Wu, J., Wang, H., Wang, S., 2020. Structural characterization of a heteropolysaccharide from fruit of *Chaenomeles speciosa* (Sweet) Nakai and its antitumor activity. *Carbohydr. Polym.* 236, 116065.
- Cui, D., Ma, J., Liang, T., Sun, L., Meng, L., Liang, T., Li, Q., 2019. Selenium nanoparticles fabricated in laminarin polysaccharides solutions exert their cytotoxicities in HepG2 cells by inhibiting autophagy and promoting apoptosis. *Int. J. Biol. Macromol.* 137, 829–835.
- Cesaretti, M., Luppi, E., Maccari, F., Volpi, N., 2003. A 96-well assay for uronic acid carbazole reaction. *Carbohydr. Polym.* 54, 59–61.
- Dubois, M., K. Gilles, A., Hamilton, J.K., Rebers, P.A., Smith, F., 1956. Colorimetric method for determination of sugars and related substances. *Anal. Chem.* 28, 350–356.
- Ferrara, N., Gerber, H.P., LeCouter, J., 2003. The biology of VEGF and its receptors. *Nat. Med.* 9, 669–676.
- Guo, L., Cui, J., Wang, H., Medina, R., Zhang, S., Zhang, X., Zhuang, Z., Lin, Y., 2021. Metformin enhances anti-cancer effect of cisplatin in meningioma through AMPK-mTOR signaling pathways. *Mol. Ther. Oncolytics.* 20, 119–131.
- Honda, S., Akao, E., Suzuki, S., Okuda, M., Kakehi, K., Nakamura, J., 1989. High-performance liquid chromatography of reducing carbohydrates as strongly ultraviolet-absorbing and electrochemically sensitive 1-phenyl-3-methyl-5-pyrazolone derivatives. *Anal. Biochem.* 180, 351–357.
- Hu, Q., Lu, Y., Luo, Y., 2021. Recent advances in dextran-based drug delivery systems: From fabrication strategies to applications. *Carbohydr. Polym.* 264, 117999.
- Kumar Varma, C.A., Jayaram Kumar, K., 2017. Structural, functional and pH sensitive release characteristics of water-soluble polysaccharide from the seeds of *Albizia lebeck* L. *Carbohydr. Polym.* 175, 502–508.
- Li, Y., Zheng, X., Chu, Q., 2021a. Bio-based nanomaterials for cancer therapy. *Nano Today.* 38, 101134.
- Li, Z., An, L., Zhang, S., Shi, Z., Bao, J., Tuerhong, M., Abudukeremu, M., Xu, J., Guo, Y., 2021b. Structural elucidation and immunomodulatory evaluation of a polysaccharide from *Stevia rebaudiana* leaves. *Food Chem.* 364, 130310.
- Li, Y., Ma, J., Song, Z., Zhao, Y., Zhang, H., Li, Y., Xu, J., Guo, Y., 2021c. The antitumor activity and mechanism of a natural diterpenoid from *Casaria graveolens*. *Front. Oncol.* 11, 688195.
- Li, J., Shen, B., Nie, S., Duan, Z., Chen, K., 2019a. A combination of selenium and polysaccharides: Promising therapeutic potential. *Carbohydr. Polym.* 206, 163–173.
- Li, Q., Chen, T., Yang, F., Liu, J., Zheng, W., 2010. Facile and controllable one-step fabrication of selenium nanoparticles assisted by L-cysteine. *Mater. Lett.* 64, 614–617.
- Li, H., Liu, D., Li, S., Xue, C., 2019. Synthesis and cytotoxicity of selenium nanoparticles stabilized by  $\alpha$ -D-glucan from *Castanea mollissima* Blume. *Int. J. Biol. Macromol.* 129, 818–826.
- Liao, W., Zhang, R., Dong, C., Yu, Z., Ren, J., 2016. Novel walnut peptide-selenium hybrids with enhanced anticancer synergism: facile synthesis and mechanistic investigation of anticancer activity. *Int. J. Nanomed.* 11, 1305–1321.
- Liu, J., Chen, Q., Feng, L., Liu, Z., 2018. Nanomedicine for tumor microenvironment modulation and cancer treatment enhancement. *Nano Today.* 21, 55–73.
- Liu, Z., Wang, K., Wang, T., Wang, Y., Ge, Y., 2022a. Copper nanoparticles supported on polyethylene glycol-modified magnetic Fe<sub>3</sub>O<sub>4</sub> nanoparticles: Its anti-human gastric cancer investigation. *Arabian J. Chem.* 15, 103523.
- Liu, G., Yang, X., Zhang, J., Liang, L., Miao, F., Ji, T., Ye, Z., Chu, M., Ren, J., Xu, X., 2021. Synthesis, stability and anti-fatigue activity of selenium nanoparticles stabilized by *Lycium barbarum* polysaccharides. *Int. J. Biol. Macromol.* 179, 418–428.
- Liu, J., Peng, Y., Wei, W., 2022b. Cell cycle on the crossroad of tumorigenesis and cancer therapy. *Trends Cell Biol.* 32, 30–40.
- Ma, Z., Li, J., Lin, K., Ramachandran, M., Zhang, D.L., Showalter, M., De Souza, C., Lindstrom, A., Solano, L.N., Jia, B., Urayama, S., Duan, Y., Fiehn, Q., Lin, T., Li, M., Li, Y., 2020. Pharmacophore hybridisation and nanoscale assembly to discover self-delivering lysosomotropic new-chemical entities for cancer therapy. *Nat. Commun.* 11, 4615.
- Nawrocka, A., Charget, M.S., Mis, A., Wilczewska, A.Z., Markiewicz, K.H., 2017. Effect of dietary fibre polysaccharides on structure and thermal properties of gluten proteins-A study on gluten dough with application of FT-Raman spectroscopy. TGA and DSC. *Food Hydrocolloids.* 69, 410–421.
- Pandit, S., Dutta, D., Nie, S., 2020. Active transcytosis and new opportunities for cancer nanomedicine. *Nat. Mater.* 19, 478–480.
- Qiao, L., Dou, X., Yan, S., Zhang, B., Xu, C., 2020. Biogenic selenium nanoparticles synthesized by *Lactobacillus casei* ATCC 393 alleviate diquat-induced intestinal barrier dysfunction in C57BL/6 mice through their antioxidant activity. *Food Funct.* 11, 3020–3031.
- Shi, J., Kantoff, P.W., Wooster, R., Farokhzad, O.C., 2017. Cancer nanomedicine: progress, challenges and opportunities. *Nat. Rev. Cancer.* 17, 20–37.
- Song, X., Qiao, L., Yan, S., Chen, Y., Dou, X., Xu, C., 2021. Preparation, characterization, and *in vivo* evaluation of anti-inflammatory activities of selenium nanoparticles synthesized by *Kluyveromyces lactis* GG799. *Food Funct.* 12, 6403–6415.
- Tang, S., Wang, T., Jiang, M., Huang, C., Lai, C., Fan, Y., Yong, Q., 2019. Construction of arabinogalactans/selenium nanoparticles composites for enhancement of the antitumor activity. *Int. J. Biol. Macromol.* 128, 444–451.
- Tang, L., Luo, X., Wang, M., Wang, Z., Guo, J., Kong, F., Bi, Y., 2021. Synthesis, characterization, *in vitro* antioxidant and hypoglycemic activities of selenium nanoparticles decorated with polysaccharides of *Gracilaria lemaneiformis*. *Int. J. Biol. Macromol.* 193, 923–932.
- Wang, T., Luo, Y., 2019. Biological fate of ingested lipid-based nanoparticles: current understanding and future directions. *Nanoscale.* 11, 11048–11063.
- Wang, L., Li, C., Huang, Q., Fu, X., 2019. Biofunctionalization of selenium nanoparticles with a polysaccharide from *Rosa roxburghii* fruit and their protective effect against H<sub>2</sub>O<sub>2</sub>-induced apoptosis in INS-1 cells. *Food Funct.* 10, 539–553.
- Wusigale, Wang, T., Hu, Q., Xue, J., Khan, M.A., Liang, L., Luo, Y., 2021. Partition and stability of folic acid and caffeic acid in hollow zein particles coated with chitosan. *Int. J. Biol. Macromol.* 183, 2282–2292.
- Xia, X., Zhang, X., Liu, M., Duan, M., Zhang, S., Wei, X., Liu, X., 2021. Toward improved human health: Efficacy of dietary selenium on immunity at the cellular level. *Food Funct.* 12, 976–989.

- Xiao, Y., Huang, Q., Zheng, Z., Guan, H., Liu, S., 2017. Construction of a *Cordyceps sinensis* exopolysaccharide-conjugated selenium nanoparticles and enhancement of their antioxidant activities. *Int. J. Biol. Macromol.* 99, 483–491.
- Xie, X., Zou, G., Li, C., 2015. Antitumor and immunomodulatory activities of a water-soluble polysaccharide from *Chaenomeles speciosa*. *Carbohydr. Polym.* 132, 323–329.
- Xu, D., Li, E., Karmakar, B., Awwad, N.S., Ibrahim, H.A., Hussein Osman, H.E., El-kottg, A.F., Abdel-Daimi, M.M., 2022. Green preparation of copper nanoparticle-loaded chitosan/alginate bio-composite: Investigation of its cytotoxicity, antioxidant and anti-human breast cancer properties. *Arabian J. Chem.* 15, 103228.
- Yan, S., Qiao, L., Dou, X., Song, X., Chen, Y., Zhang, B., Xu, C., 2021. Biogenic selenium nanoparticles by *Lactobacillus casei* ATCC 393 alleviate the intestinal permeability, mitochondrial dysfunction and mitophagy induced by oxidative stress. *Food Funct.* 12, 7068–7080.
- Yang, H., Sun, A., Yang, J., Cheng, H., Yang, X., Chen, H., Huanfei, D., Falahati, M., 2021a. Development of doxorubicin-loaded chitosan–heparin nanoparticles with selective anticancer efficacy against gastric cancer cells *in vitro* through regulation of intrinsic apoptosis pathway. *Arabian J. Chem.* 14, 103266.
- Yang, J., Wang, J., Huang, K., Zhu, M., Liu, Q., Liu, G., Qin, S., 2021b. Selenium enriched *Bacillus subtilis* yb-1 114246 activated the TLR2–NF- $\kappa$ B1 signaling pathway to regulate chicken intestinal  $\beta$ -defensin 1 expression. *Food Funct.* 12, 5913–5926.
- Ye, M.J., Xu, Q.L., Tang, H.Y., Jiang, W.Y., Su, D.X., He, S., Zeng, Q.Z., Yuan, Y., 2020. Development and stability of novel selenium colloidal particles complex with peanut meal peptides. *Lwt.* 126, 109280.
- Yu, J., Dong, X., Jiao, J., Yu, S., Ji, H., Liu, A., Chen, Y., 2022. The inhibitory effects of selenium nanoparticles modified by fructose-enriched polysaccharide from *Codonopsis pilosula* on HepG2 cells. *Ind. Crops Prod.* 176, 114335.
- Zeng, Y., Xiang, Y., Sheng, R., Tomás, H., Rodrigues, J., Gu, Z., Zhang, H., Gong, Q., Luo, K., 2021. Polysaccharide-based nanomedicines for cancer immunotherapy: A review. *Bioact. Mater.* 6, 3358–3382.
- Zeng, D., Zhao, J., Lu, K.H., Cheung, S.T., Wong, K.H., Chen, T., 2019. Potentiation of *in vivo* anticancer efficacy of selenium nanoparticles by mushroom polysaccharides surface decoration. *J. Agric. Food Chem.* 67, 2865–2876.
- Zhang, X., Zhang, L., Xia, K., Dai, J., Huang, J., Wang, Y., Jia, Y., 2022. Effects of dietary selenium on immune function of spleen in mice. *J. Funct. Foods.* 89, 104914.
- Zhang, Y., Li, X., Huang, Z., Zheng, W., Fan, C., Chen, T., 2013. Enhancement of cell permeabilization apoptosis-inducing activity of selenium nanoparticles by ATP surface decoration. *Nanomed-Nanotechnol.* 9, 74–84.
- Zhang, J., Song, Z., Li, Y., Zhang, S., Bao, J., Wang, H., Dong, C.X., Ohizumi, Y., Xu, J., Guo, Y., 2021a. Structural analysis and biological effects of a neutral polysaccharide from the fruits of *Rosa laevigata*. *Carbohydr. Polym.* 265, 118080.
- Zhang, Y., Zeng, Y., Cui, Y., Liu, H., Dong, C., Sun, Y., 2020a. Structural characterization, antioxidant and immunomodulatory activities of a neutral polysaccharide from *Cordyceps militaris* cultivated on hull-less barley. *Carbohydr. Polym.* 235, 115969.
- Zhang, W.H., Wu, J., Weng, L., Zhang, H., Zhang, J., Wu, A.W., 2020b. An improved phenol-sulfuric acid method for the determination of carbohydrates in the presence of persulfate. *Carbohydr. Polym.* 227, 115332.
- Zhang, S., Song, Z., Shi, L., Zhou, L., Zhang, J., Cui, J., Li, Y., Jin, D. Q., Ohizumi, Y., Xu, J., Guo, Y., 2021b. A dandelion polysaccharide and its selenium nanoparticles: Structure features and evaluation of anti-tumor activity in zebrafish models. *Carbohydr. Polym.* 270, 118365.
- Zhang, J., Teng, Z., Yuan, Y., Zeng, Q., Lou, Z., Lee, S.H., Wang, Q., 2018. Development, physicochemical characterization and cytotoxicity of selenium nanoparticles stabilized by beta-lactoglobulin. *Int. J. Biol. Macromol.* 107, 1406–1413.
- Zhang, X., Song, Z., Li, Y., Wang, H., Zhang, S., Reid, A.M., Lall, N., Zhang, J., Wang, C., Lee, D., Ohizumi, Y., Xu, J., Guo, Y., 2021c. Cytotoxic and antiangiogenic xanthenes inhibiting tumor proliferation and metastasis from *Garcinia xipshuanbannaensis*. *J. Nat. Prod.* 84, 1515–1523.
- Zhang, S., Zhang, H., Shi, L., Li, Y., Tuerhong, M., Abudukeremu, M., Cui, J., Li, Y., Jin, D.Q., Xu, J., Guo, Y., 2021d. Structure features, selenylation modification, and improved anti-tumor activity of a polysaccharide from *Eriobotrya japonica*. *Carbohydr. Polym.* 273, 118496.
- Zhou, K., Taoerdahong, H., Bai, J., Bakasi, A., Wang, X., Dong, C., 2020. Structural characterization and immunostimulatory activity of polysaccharides from *Pyrus sinkiangensis* Yu. *Int. J. Biol. Macromol.* 157, 444–451.
- Zhou, L., Song, Z., Zhang, S., Li, Y., Xu, J., Guo, Y., 2021. Construction and antitumor activity of selenium nanoparticles decorated with the polysaccharide extracted from *Citrus limon* (L.) Burm. f. (Rutaceae). *Int. J. Biol. Macromol.* 188, 904–913.